Catalysis Science & Technology

Accepted Manuscript

This article can be cited before page numbers have been issued, to do this please use: X. Wang, J. Wang, A. Liu, Y. Yu, J. Ji, K. Guo, H. Wan, C. Tang and L. Dong, *Catal. Sci. Technol.*, 2020, DOI: 10.1039/D0CY00191K.

ROYAL SOCIETY OF CHEMISTRY

rsc.li/catalysis

View Article Online
DOI: 10.1039/D0CY00191K

ARTICLE

Unravelling the structure sensitivity of CuO/SiO_2 catalysts in NO + CO reaction

Received 00th January 20xx,
Accepted 00th January 20xx

DOI: 10.1039/x0xx00000x

Xiuwen Wang,[a] Jin Wang,[a] Annai Liu,[a] Yaxin Yu,[a] Jiawei Ji,[a] Kai Guo,[a] Haiqin Wan,[bc] Changjin Tang*[ab] and Lin Dong[abc]

CuO/SiO_2 catalysts with vast difference in copper dispersion were prepared by impregnation (denoted as CuSi-IM) and ammonia-evaporation (denoted as CuSi-AE) methods and tested for NO reduction by CO. Despite the inferior dispersion of copper species in CuSi-IM catalysts, they exhibited significantly higher NO conversion efficiency, with more than one order of activity enhancement achieved in comparison with CuSi-AE samples. Ex situ XRD, in situ DRIFTS, and CO-TPR characterizations were carried out to study the nature of active copper species and their evolution under reaction conditions. A clear dispersion-dependent reduction behavior (for CuSi-AE, step-wise reduction; for CuSi-IM, one step reduction) under CO atmosphere was observed, and the generation of Cu^0 preferentially occurred at lower temperatures for CuSi-IM samples, which accounted for the better performance in NO+CO reaction. Lastly, NO-TPD and TPSR experiments were operated and the essential role of Cu^0 in promoting NO dissociation was proposed. The results of present study would deepen our understanding on the reaction behaviors of copper catalysts in NO + CO reaction.

1. Introduction

As one of the main atmospheric pollutants, nitrogen oxides (NO_x) is an important cause of many environmental problems such as photochemical smog and acid rain[1, 2]. It is well acknowledged that the concentration of nitrogen oxides emitted from fuel combustion in transportation (mobile source) and industrial processes (stationary source) is relatively high and needs to be tightly controlled. Catalytic elimination is a mature strategy for reducing nitrogen oxide emission. Among various reductants, CO is notable not only for its high conversion efficiency, but also due to the fact that in many cases, they co-exist with NO in the exhaust as a result of incomplete combustion of fuels. Hence, the using of CO as a reductant to convent NO to N_2 shows attractive advantage of low cost and no need for extra reductant. As such, the reaction of NO reduction by CO has been extensively studied[3-5]. Previous investigations paid substantial attention on supported noble metal (Pt, Pd, Ru, Rh) catalysts due to their superior catalytic activity and selectivity[6-8]. However, such catalysts exhibit some deficiencies like high cost, low reserves, and poor thermal stability[9]. Therefore, researchers have turned their attention to alternatives of noble metals, and transition metal oxides show attractive prospects[10, 11].

CuO is generally used as an active component, and exhibits superior performance in NO+CO reaction[12-16]. Centi et al. showed copper oxide was among the most active transition metal oxide catalysts for NO+CO reaction[17]. It is well known that to obtain an improved performance, the control of interaction between copper species and the underlined support is important. For example, Liu et al. studied the morphology effect of support on the reactivity of CuO/CeO_2 catalysts[18]. They found the surface effect led to higher NO conversion for CuO/CeO_2 nanorods, while CuO supported on ceria polyhedra and cubes were less active. Sun et al. explored the CuO catalysts supported on pure anatase TiO_2 and ZrO_2-doped TiO_2 (TZ) [19]. Copper oxides supported on the TZ were much easier to be reduced and had stronger adsorption stability of NO_x than those supported on the pure TiO_2. Thus, the ZrO_2-doped catalysts showed superior activity and selectivity to common Cu-TiO_2 catalysts. On the other hand, the tune of chemical state of copper species is another way to regulate the performance. Takashi et al. investigated the active species of CuO/γ-Al_2O_3 catalysts, and they proposed that the isolated Cu^{2+} was the active species while aggregated CuO species would significantly reduce the activity of NO reduction[20]. However, Jiang et al. found that when excess copper was supported on γ-Al_2O_3, a continuous increase of activity was observed with the formation of crystalline CuO[21]. Jang et al. used TiO_2 as carrier, and examined the Cu oxidation states on the catalysis of NO+CO by adjusting pretreatment atmosphere[22]. It was found that NO decomposition was better by low-valence Cu species than by high-valence Cu species, i.e. $Cu^0 > Cu^+ > Cu^{2+}$. Haller et al. claimed that the concentration of

[a] School of Chemistry and Chemical Engineering, Nanjing University, Nanjing 210023, China.
[b] Jiangsu Key Laboratory of Vehicle Emissions Control, Nanjing 210023, China.
[c] School of Environment, Nanjing University, Nanjing 210023, China.
* Corresponding author:
E-mail address: tangcj@nju.edu.cn (C. Tang).

View Article Online
DOI: 10.1039/D0CY00191K

Cu^+ species ran parallel to the NO conversion and the rate-determining step of the NO reduction with CO was likely to be the NO dissociation over Cu^+ species[23]. From these results, we can know that no consensus has been achieved regarding which kind of copper species is the active sites in NO + CO reaction.

To have a fundamental understanding about role of copper species in NO+CO, the interference from support effect should be excluded. In other words, the support itself should be chemical inertness. In NO+CO reaction, NO dissociation on a copper surface is unaffected by SiO_2 support[24]. Thus, SiO_2 is a suitable and ideal support for investigation. Previous studies have reported CuO supported SiO_2 catalysts can be prepared by impregnation[25], deposition-precipitation[26], ionic exchange[27], sol-gel[28]. By conventional methods for catalyst preparation such as impregnation, bulk CuO is easily formed on the surface of SiO_2 even at a low loading amount[29]. Recently, some studies have reported an ammonia-evaporation method which could graft copper species with high loadings on the surface of SiO_2 support without appearance of crystalline CuO[29, 30]. Thus, dispersed CuO and bulk CuO species with same loading amounts can be achieved in CuO/SiO_2 catalyst by ammonia-evaporation method (AE) and impregnation method (IM). From this point of view, in this paper, we used the above two methods to prepare the CuO/SiO_2 catalysts with a series of CuO loadings and applied them in NO+CO reaction. Comparative studies found that CuO/SiO_2 catalyst with bulk CuO on the surface has much better activity. Through a series of characterizations, it was found that Cu^0 was the active center of the reaction, and because the bulk CuO was more easily reduced to Cu^0 by CO, it exhibited favorable catalytic activity. The interaction between reactants and the catalysts were further analyzed to explain the results of such experiments.

2. Experimental section

2.1 Materials

Silica gel, $Cu(NO_3)_2{\cdot}3H_2O$, and 28% ammonia aqueous were of analytical grade, and were purchased from Sinopharm Chemical Reagent, Co., Ltd., China without further treatment.

2.2 Catalysts preparation

Before used, SiO_2 was calcined in flowing air at 450 °C for 4 h under an air atmosphere. CuO/SiO_2-IM samples were prepared by wet impregnation method. SiO_2 was added into a $Cu(NO_3)_2$ aqueous solution. After stirring, the mixture solution was evaporated at 100 °C for removing the water. Then, the material was dried overnight at 120 °C and calcined at 450 °C for 4 h. CuO/SiO_2-AE samples were prepared by ammonia-evaporation method. First, an excessive amount of ammonia aqueous was added dropwise to a $Cu(NO_3)_2$ aqueous solution and stirred for 30 min. Then, SiO_2 was added into the mixture solution and stirred for 4 h. Subsequently, the suspension was evaporated to remove ammonia and lower the pH of the solution to 6-7. The as-prepared material was washed with ethanol and deionized water and then dried overnight at 120 °C. Finally, the catalysts were calcined at 450 °C for 4 h. The loading amounts of CuO were 5 wt%, 20 wt%, 30 wt%, and 40 wt%, respectively. For the sake of simplicity, the resulting catalysts were represented by CuSi1-AE/IM, CuSi2-AE/IM, CuSi3-AE/IM, and CuSi4-AE/IM.

2.3 Catalysts Characterization

X-ray diffraction (XRD) patterns were obtained via a Philips X'pert Pro diffractometer using Ni-filtered Cu Kα radiation (0.15 nm). The recording range was from 10° to 80° and operated at 40 kV and 40 mA.

The morphology of samples was analyzed by using a JEOL JEM-2100 transmission electron microscope (TEM). The acceleration voltage was 200 kV.

The actual Cu^{2+} loadings were measured on a PE Optima 5300DV inductively coupled plasma optical emission spectrometer (ICP-OES).

Brunauer-Emmett-Teller (BET) surface areas were determined by a nitrogen adsorption at 77 K on a Micrometrics ASAP-2020 adsorption analyzer. Each sample was degassed at 300 °C for 3 h before analysis.

Fourier transform Infrared (FT-IR) spectra were collected on a Nicolet IS10 FT-IR spectrometer at a spectral resolution of 2 cm^{-1} for 32 scans. The background was collected first and then subtracted for every sample.

X-ray photoelectron spectroscopy (XPS) analysis was carried out on a PHI 5000 Versa Probe system. The charging effect of the sample was compensated by calibrating all the binding energies with the adventitious C 1s peak at 284.6 eV.

CO temperature programmed reduction (CO-TPR) experiments were performed by an online LC-D series mass spectrometer. Prior to reduction, the catalyst (50 mg) was pretreated in He stream. After that, CO-He (10% of CO by volume) was switched on until the adsorption was saturated, and then the sample was heated from ambient temperature to 650 °C at a rate of 10 °C·min^{-1}. The discharged CO and CO_2 gases were collected by mass spectrometer.

H_2-temperature programmed reduction (H_2-TPR) was carried out by a thermal conductivity detector. Prior to reduction, 10 mg of the catalyst loaded in a quartz U-tube was pretreated in N_2 stream at 200 °C for 0.5 h. After that, the sample was heated from room temperature to 600 °C at a rate of 10 °C·min^{-1} in a mixed H_2-Ar (7% of CO by volume) stream.

View Article Online
DOI: 10.1039/D0CY00191K

In situ diffuse reflectance infrared Fourier transform spectra (in situ DRIFTS) were performed by a Nicolet 5700 FT-IR spectrometer at a spectral resolution of 4 cm^{-1}. Prior to testing, the sample was purged by N_2 stream at 450 °C for 0.5 h. The background spectrum was then collected at ambient temperature. Thereafter, a mixture flow of 10 vol% CO and 90 vol% He was introduced to the sample at a flow rate of 5 $mL{\cdot}min^{-1}$ for 30 min to achieve saturation. The weakly adsorbed CO was purged with N_2, and the CO adsorption spectrum was collected. To investigate the CO adsorption after CO pretreatment, the sample was first exposed to CO-He for 10 min at different target temperatures, then cooled to ambient temperature and finally subjected to CO adsorption, N_2 purge and adsorption spectrum collection steps.

NO temperature programmed desorption (NO-TPD) experiment was carried out. About 50 mg of the sample was purged in a He stream at 200 °C for 1 h. Afterwards, the sample was exposed to NO (50 $mL{\cdot}min^{-1}$) at ambient temperature until the adsorption was saturated. Subsequently, purged the sample with the flowing high purified He (50 $mL{\cdot}min^{-1}$) to remove gaseous and weakly adsorbed NO. Finally, the sample was heated to 600 °C at a rate of 10 $°C{\cdot}min^{-1}$ for NO desorption. NO and N_2O were recorded using a Nicolet IS10 FTIR spectrometer, And N_2 were recorded using a mass spectrometer.

Temperature programmed surface reaction (TPSR) was performed by a Nicolet IS10 FTIR spectrometer. The sample (50 mg) was loaded into a quartz tube and pretreated with a high purified He stream at 200 °C for 30 min. The sample was then cooled to 150 °C. At that temperature, NO gas was flowed in until saturation, and the weakly adsorbed NO was removed by high purified He (50 $mL{\cdot}min^{-1}$). Finally, CO-He (10% of CO by volume) was switched on and the signals at different times were continuously collected.

2.4 Catalytic performance tests

The catalyst (50 mg) was used for testing under steady state at a space velocity of 12 000 $mL{\cdot}g^{-1}h^{-1}$. The reaction gas was composed of NO-He (5% of NO by volume) and CO-He (10% of CO by volume) with a total flow rate of 10 $mL{\cdot}min^{-1}$. A flowing He stream was applied to remove impurities on the surface of catalyst at 200 °C for 0.5 h. After that, the sample was exposed to the reactant gas until saturation adsorption was achieved. Then, the reaction was carried out at each target temperature. The concentration of N_2, NO, and CO were detected by a column packed with 5A and 13× molecular sieves and a thermal conduction detector. Values of percentage conversion and production yield are defined as follows:

NO conversion = $([NO]_{in} - [NO]_{out})/[NO]_{in} \times 100\%$

N_2 yield = $2[N_2]_{out}/[NO]_{in} \times 100\%$

Where $([NO]_{in}$, $[NO]_{out}$ and $[N_2]_{out}$ are the molar flow of the inlet or outlet gas.

3. Results and discussion

3.1. Structural characteristics

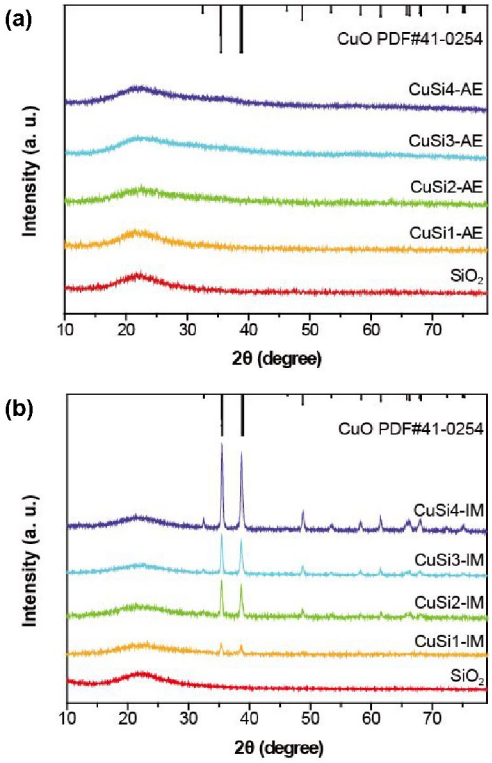

Fig. 1 XRD results of (a) CuSi-AE, and (b) CuSi-IM samples.

Fig. 1 displays the XRD patterns of CuO/SiO_2 catalysts. It is obvious the preparation methods have great influence on the dispersion state of copper species. CuSi-AE samples with different CuO contents only show a broad peak of amorphous SiO_2, with no any signal from CuO, demonstrating that Cu species are well dispersed or too small to be detected on the SiO_2 support when synthesized by ammonia-evaporation method. In contrast, the conventional CuSi-IM samples exhibit characteristic peaks of CuO with sharp intensity at 2θ = 35.5°, 38.7°, 38.9°, and 48.7°, indicating that bulk crystalline CuO (JCPDS: 41-0254) forms on the surface of SiO_2 even with the lowest nominal content of 5 wt%, and the intensity of diffraction peaks increases with CuO loadings due to the growth of CuO particles. The morphologies of as-prepared catalysts were observed by TEM characterization. As exhibited in **Fig. 2**, the copper species in CuSi2-AE catalyst are distributed uniformly over the SiO_2 support, and no particle can be observed. In the case of CuSi2-IM catalyst, aggregated

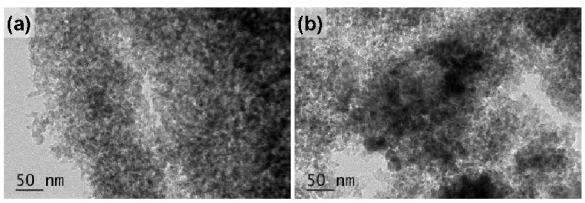

Fig. 2 TEM images of (a) CuSi2-AE, and (b) CuSi2-IM samples.

View Article Online
DOI: 10.1039/D0CY00191K

Table 1 Physicochemical properties of CuSi-AE and CuSi-IM samples.

Catalysts	Cu^{2+} loaded (wt%)	Cu^{2+} detected (wt%)	Surface area (m^2g^{-1})	Pore volume (cm^3g^{-1})	Pore size (nm)
CuSi1-AE	5	4.1	264.6	0.84	9.8
CuSi2-AE	20	14.6	318.1	0.74	7.2
CuSi3-AE	30	21.5	374.3	0.66	5.4
CuSi4-AE	40	23.0	286.5	0.63	7.1
CuSi1-IM	5	4.1	287.1	0.86	9.1
CuSi2-IM	20	15.5	262.6	0.80	9.1
CuSi3-IM	30	21.6	245.3	0.75	9.1
CuSi4-IM	40	36.2	213.5	0.62	8.8

CuO crystallites are observed, supporting the observation made by XRD.

The actual concentrations of Cu species in the as-synthesized catalysts were characterized by ICP analysis and results were listed in **Table 1**. It can be found that except for the sample with excessive introduced copper (40 wt%), the actual copper loadings are comparable for both methods. It also shows that unlike the conventional impregnation method, the actual loading amounts of copper for CuSi-AE will reach a saturation, and do not exhibit a continuous increase with the further increase of $Cu(NO_3)_2$ precursor, probably as a result of limited grafting sites on silica surface.

The N_2 adsorption-desorption isotherms of CuO/SiO_2 samples and their pore size distribution curves were plotted in **Fig. 3**. All samples reveal a type Ⅳ Langmuir adsorption isotherm according to the IUPAC classification, indicating the existence of mesoporous structure. The average pore diameters of CuSi-AE samples decrease from 10.6 nm to 6.5 nm with CuO loadings, while CuSi-IM samples exhibit similar pore diameters centered at 9.2 nm. The BET surface area, pore volume, and average pore size were summarized in **Table 1**. It is found that with the CuO loading amounts increase from 5 to 30 wt%, the BET surface area of CuSi-AE samples increases gradually, probably as a result of the strong interaction between copper species and SiO_2 framework in ammonia solution and the formation of copper phyllosilicate with layered structure[26, 31]. Unlike the CuSi-AE samples, the parameter of CuSi-IM samples decreases with CuO loadings, which can be reasonably linked to the poor dispersion of CuO[32].

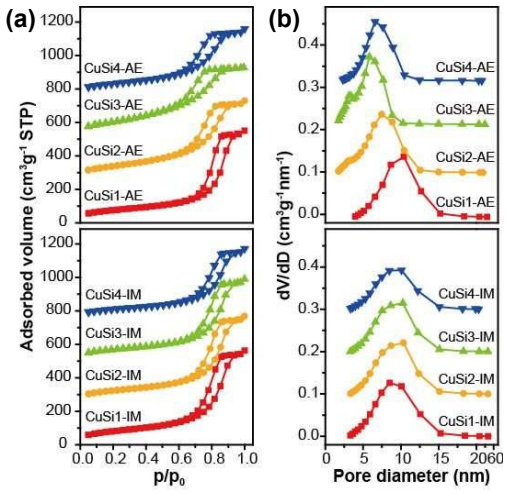

Fig. 3 N_2 adsorption-desorption isotherms (a) and pore size distribution curves (b) of CuSi-AE and CuSi-IM samples.

It was previously reported that by using the ammonia evaporation method to deposit copper species on silica surface, the copper species can be grafted on silica matrix generating copper phyllosilicate structure[33]. To confirm the species, IR characterization was operated. As presented in **Fig. 4**, CuSi-AE samples as well as CuSi-IM samples all show two characteristic bands at approximately 800 and 1054 cm^{-1} ascribed to the ν_{SiO} symmetric and asymmetric stretching vibration of SiO_2, respectively[30, 34]. For CuSi-AE samples, the additional appearance of the δ_{OH} vibration at near 670 cm^{-1} suggest the formation of copper phyllosilicate, which is absent in the spectra of CuSi-IM samples[35]. XPS spectra of CuSi2-AE and

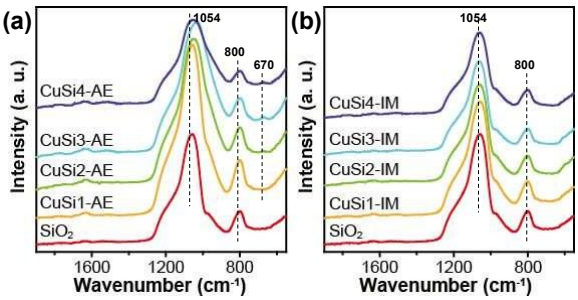

Fig. 4 IR spectra of (a) CuSi-AE and (b) CuSi-IM samples.

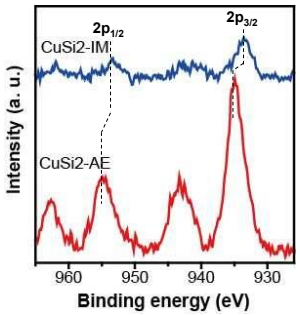

Fig. 5 Cu 2p spectra of CuSi2-AE and CuSi2-IM samples.

View Article Online
DOI: 10.1039/D0CY00191K

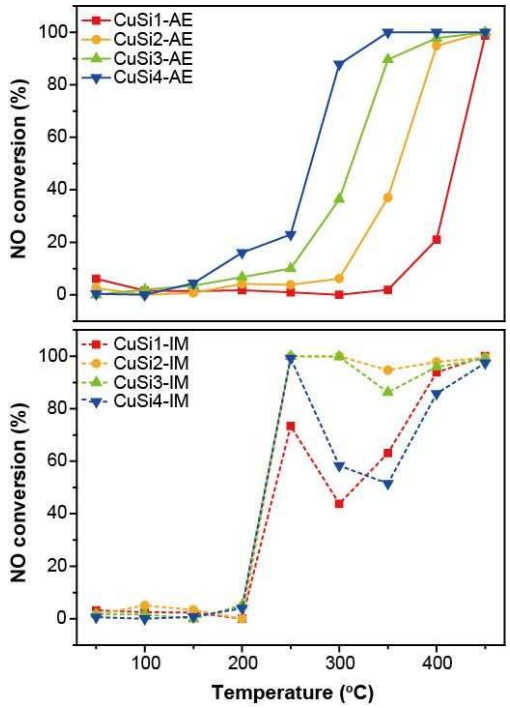

Fig. 6 NO conversion of CuSi-AE and CuSi-IM samples as a function of the reaction temperature.

CuSi2-IM were provided as an example to further determine the existence state of Cu species (**Fig. 5**). It is obvious that for the Cu $2p_{3/2}$ and Cu $2p_{1/2}$ region, the characteristic peaks at 934.9 eV and 955.0 eV for CuSi2-AE and at 933.5 eV and 953.5 eV for CuSi2-IM are detected, indicating that Cu species mainly exist as Cu^{2+} [26, 36]. And an apparent shift of Cu 2p peak to positive value for CuSi2-AE manifests the strong interaction between Cu species and SiO_2 support[37]. Moreover, the intensity of Cu 2p signal for CuSi2-AE is much stronger than that for CuSi2-IM, in good agreement with the high dispersion nature of copper species in CuSi-AE samples.

3.2. The catalytic performance of NO + CO reaction

The catalytic performance of CuO/SiO_2 samples in the reaction of NO reduction by CO was shown in **Fig. 6**. For CuSi-AE samples, the catalytic activity increased with increasing Cu loadings, indicating that the catalyst with a higher concentration of Cu species on the surface contributes to the improvement of catalytic activity. However, a saturated value of NO conversion will occur as Cu content increases in CuSi-IM samples. Among them, CuSi2-IM with 15 wt% Cu^{2+} loading amount exhibits the best catalytic performance, demonstrating that the catalyst with proper amount of aggregated CuO can promote the NO+CO performance. For all the catalysts at reaction temperature below 200 °C, poor reactivity is exhibited, with NO conversion of less than 20%. However, when the temperature is increased to higher than 200 °C, dramatic enhancement of activity is observed, and this is particularly true for CuSi-IM catalysts. For example, the activity of CuSi-IM series catalysts is less than 5% at 200 °C, but realize full conversion of NO when the reaction temperature is increased to 250 °C. For the two kinds of CuO/SiO_2 catalysts, it is obviously the catalytic performance of CuSi-IM samples increases more obviously than CuSi-AE samples with the amount of CuO increases, following the order of CuSi4-IM = CuSi3-IM = CuSi2-IM > CuSi1-IM > CuSi4-AE > CuSi3-AE > CuSi2-AE > CuSi1-AE. Further increasing the temperature contributes to the continuous increase in the activity of CuSi-AE samples, but the activity of CuSi-IM samples exhibits an unexpected decline. This is extraordinary because usually the catalytic performance shows a positive response with temperature increase. N_2 yields have the same order as the NO conversion here (**Fig. S1**). Referring to the above BET results which are not related to catalytic performance, it is clear that the surface area is not the main factor affecting activity. Thus, to understand the differences in surface structure and the resulting changes in chemical properties, a series of characterizations of the catalysts were carried out in the following sections.

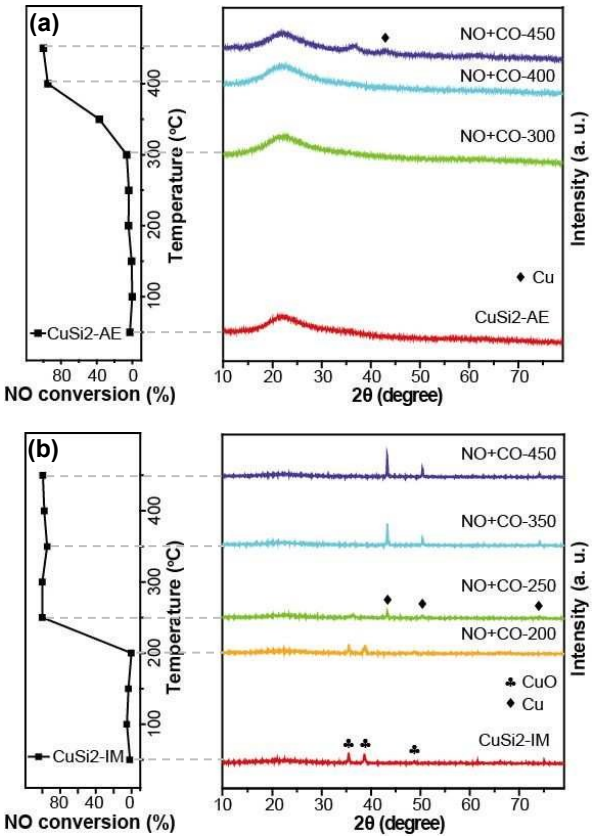

Fig. 7 NO conversion and corresponding XRD results as a function of reaction temperature of (a) CuSi2-AE, and (b) CuSi2-IM sample.

3.3. Chemical properties of surface copper species

Since the reaction atmosphere contains CO, it is expected the presence of CO can induce some structural variations on CuO/SiO_2 catalysts. To investigate any changes of catalysts during the reaction, CuSi2-IM with optimal performance and the corresponded CuSi2-AE sample were selected for XRD test

View Article Online
DOI: 10.1039/D0CY00191K

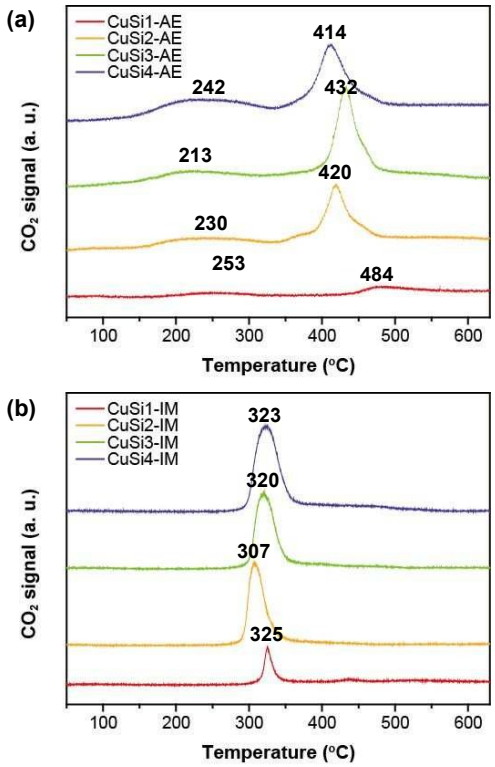

Fig. 8 CO-TPR patterns of (a) CuSi-AE and (b) CuSi-IM samples.

(**Fig. 7**). For CuSi2-AE, no characteristic peak of crystalline phase appears until the reaction temperature reaches 450 °C. When the temperature gets to 450 °C, the characteristic peak of Cu can be detected, indicating the reduction of CuO and the aggregation of Cu species in the reaction atmosphere during the heating process. In contrast, for CuSi2-IM, when the reaction temperature rises to 250 °C, the peak of CuO disappears, and at the same time, the peak of Cu^0 appears. By comparing the result of ex-situ XRD and activity profile (**Fig. 7**), it declares that the temperature point corresponding to the characteristic peak of Cu^0 is also the point at which the reaction activity is significantly improved. From this it can be concluded that metallic Cu^0 may be the active sites of NO + CO reaction under existing reaction conditions. Furthermore, the CuO in CuSi2-IM sample is preferentially reduced to Cu^0 compared to CuSi2-AE sample, indicating the dispersion of CuO probably has an important effect on the reduction profile of Cu species[22, 38, 39].

In order to further explore the variation in Cu^0 species formation between the two samples, CO-TPR was performed and the changes of CuO species with different surface types during CO reduction treatment were detected. As shown in **Fig. 8**, it is obvious that CuSi-AE samples have two reduction peaks with centers at about 230 °C and 420 °C, respectively. One possible explanation is that the reduction of CuO in a dispersed state involves two steps: Cu^{2+} to Cu^+ and Cu^+ to Cu^0. A similar phenomenon was reported by Martinez-Arias when they examined the redox properties of CuO/Al_2O_3 by CO-TPR[40].

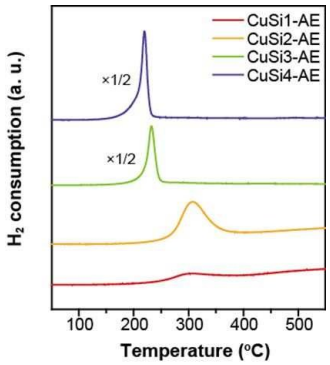

Fig. 9 H_2 temperature programmed reduction (H_2-TPR) of CuSi-AE samples.

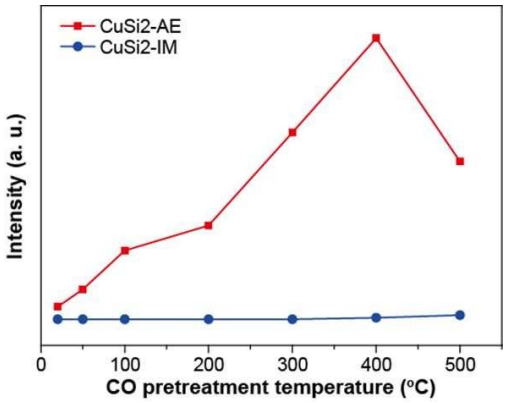

Fig. 10 Relationship between CO pretreatment temperature and integrated intensity of IR spectra for copper carbonyl over CuSi2-AE and CuSi2-IM sample.

They claimed that when the reduction temperature was below 300 °C, a small reduction was achieved, which attributed to the reduction of isolated Cu^{2+} to Cu^+ and a small amount of Cu^0. Higher CO pretreatment temperatures led to the appearance of another stronger reduction in which metallic copper particles appeared and Cu^+ gradually decreased. However, for CuSi-IM sample, it has only one reduction peak, and the corresponding temperature is about 320 °C, suggesting the occurrence of direct reduction of bulk CuO into metallic Cu^0 [38].

As we know, it is also possible that for CuSi-AE samples, they include two states of CuO on SiO_2 surface, i.e. dispersed CuO and CuO clusters. To discriminate this possibility, H_2-TPR was carried out to verify the state of CuO. As shown in **Fig. 9**, only one reduction peak displayed, which manifest that there is only dispersed CuO species existing in CuSi-AE samples. Therefore, the reduction peaks of CuSi-AE samples in CO-TPR are not concerned to the states of CuO, and are mainly related to the reduction process of $Cu^{2+} \rightarrow Cu^+ \rightarrow Cu^0$.

In-situ DRIFT spectrometer was further used to confirm the different reduction behaviors of the CuO/SiO_2 catalysts. Since CO is only irreversibly bound to Cu^+ species and easily desorbs from Cu^0 and Cu^{2+}, it can be used as a useful probe molecule for Cu^+, providing the possibility of quantitative discrimination

View Article Online
DOI: 10.1039/D0CY00191K

Table 2 Crystalline size of the prepared CuSi4-IM sample.

Reaction temperature	250 °C	300 °C	450 °C
d_{Cu} (nm)	50.7	124.7	177.0

of Cu^+ on the surface[41]. After recorded CO-Cu^+ species at room temperature with CO pretreatment at different temperatures, the peak intensity was calculated and the results as a function of CO pretreatment temperature are shown in **Fig. 10**. For CuSi2-AE, the content of Cu^+ increases as the CO pretreatment temperature increases from 30-400 °C, indicating that Cu^{2+} is gradually reduced to Cu^+ by CO pretreatment. When the pretreatment temperature is higher than 400 °C, the content of Cu^+ begins to decrease, implying that Cu^+ is further reduced to Cu^0. In contrast, the content of Cu^+ in CuSi2-IM sample is always low, suggesting that most Cu^{2+} might be directly reduced to Cu^0 without the emergence of Cu^+ intermediate species. This is consistent with the CO-TPR results above. In addition, combing these phenomena with the NO+CO activity results, it is found that the activity of CuSi2-AE does not increase with increasing Cu^+ content. For example, at 300 °C, a large amount of Cu^+ has been produced, but the NO conversion is less than 10%. However, the activity of CuSi2-IM increases from 250 °C, while the Cu^+ content do not change significantly, indicating Cu^0 species is the active site in the NO+CO reaction. Furthermore, the above results also suggest that the reduction of bulk CuO to Cu^0 is much easier than the reduction of dispersed CuO, which is the essential reason why the activity of CuSi-IM samples is better than that of CuSi-AE samples.

It has been proved that the appearance of Cu^0 is beneficial to improve the catalytic performance, but the reason for the deactivation of CuSi-IM samples at higher reaction temperatures needs further explanation. CuSi4-IM sample, which shows the most significant decrease in activity at high temperature, was selected as the target sample for the following study. According to Scherrer equation, the crystallite size of Cu^0 was calculated and summarized. As listed in **Table 2**, the crystallite size increases from 50.7 to 177.0 nm as the reaction temperature increases from 250 to 450 °C. A possible explanation for this may be that the reduced Cu species aggregate at high temperature and the particle size gradually become larger. Thus, Cu^0 with the larger particle reduces the number of active sites exposed on the catalyst surface, resulting in a marked decline in the activity of NO reduction[42].

3.4. Possible reaction mechanism for NO reduction by CO

To have further insight into the reaction, the interaction of Cu^{2+} and Cu^0 species with reactants was studied. Since CuSi-AE samples have more dispersed Cu^{2+} on the catalysts surface, CuSi2-AE (named CuSi-fresh) was chosen as the target sample of Cu^{2+} species. In addition, CuSi2-AE would produce more Cu^0 after NO+CO pretreatment at 450 °C, so it was selected as the target sample for investigating Cu^0 species (named CuSi-spent). First of all, NO temperature-programed desorption (TPD) was

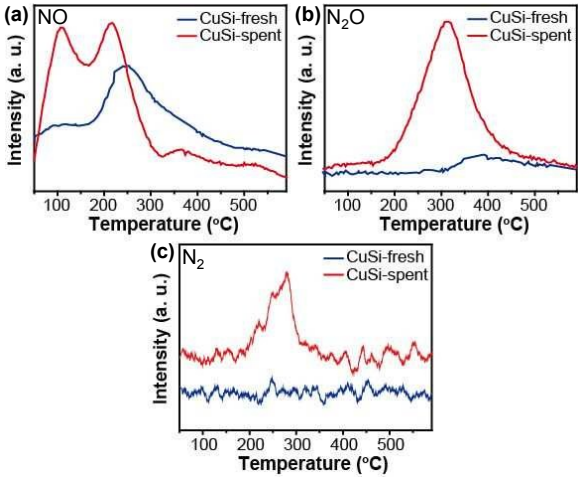

Fig. 11 NO-TPD (a, b, and c) results of CuSi-fresh and CuSi-spent samples.

chosen to help understanding the interaction between NO and the surface species of catalysts and any dissociation process of NO. All in all, NO, N_2O, and N_2 are detected. As can be seen from **Fig. 11a**, there are mainly two desorption peaks of NO, which are detected at about 120, 250 °C for CuSi-fresh, and 110, 215 °C for CuSi-spent. These desorption peaks originate from the weakly adsorbed NO species[43, 44]. It is worth noting that the desorption temperature of NO on CuSi-spent is obviously lower than that of CuSi-fresh. **Fig. 11b** shows the desorption curve of N_2O at different temperatures. N_2O is produced by the dissociation of NO. The temperature of peak center for CuSi-spent is also lower than the temperature for CuSi-fresh, which suggests that Cu^0 species are more favorable for NO dissociation. **Fig. 11c** further provides evidence for NO dissociation: the desorption signal of N_2, which is generated by the dissociation of N_2O. Moreover, the desorption amounts of NO, N_2O and N_2 for CuSi-spent are larger than that for CuSi-fresh, indicating that CuSi-spent possesses more active sites for NO adsorption.

To disclose the reactivity of these surface activated NO_x species, TPSR was further investigated (**Fig. 12**). After the

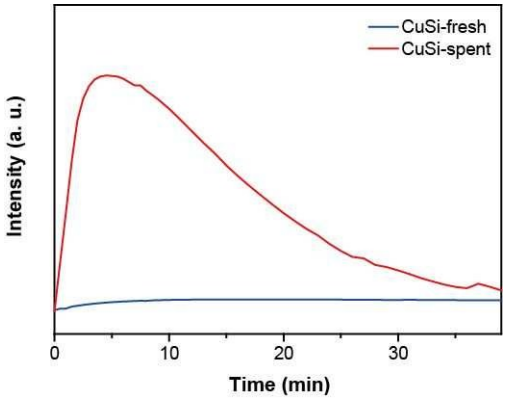

Fig. 12 TPSR result of CuSi-fresh and CuSi-spent samples at 150 °C.

View Article Online
DOI: 10.1039/D0CY00191K

adsorption of NO reached saturation at 150 °C, a CO stream was introduced. At the same time, the FTIR spectrometer was used to test the change of CO_2 content. The peak of CO_2 attributes to the combination of CO and O, where O comes from the dissociation of NO. It is clearly observed that CuSi-spent sample produces more CO_2 than CuSi-fresh, which again confirms that Cu^0 species is more active for NO decomposition.

On the basis of NO-TPD and TPSR results, a possible model for the reaction process of NO reduction by CO under the current conditions is tentatively proposed:

$NO + S \rightarrow NO_{(a)}$ (1)
$CO + S \rightarrow CO_{(a)}$ (2)
$NO_{(a)} + NO_{(a)} \rightarrow ONNO_{(a)}$ (3)
$ONNO_{(a)} \rightarrow N_2O_{(a)} + O_{(a)}$ (4)
$N_2O_{(a)} \rightarrow N_2O + S$ (5)
$N_2O_{(a)} \rightarrow N_2 + O_{(a)}$ (6)
$CO_{(a)} + O_{(a)} \rightarrow CO_2 + 2S$ (7)
$N_{(a)} + N_{(a)} \rightarrow N_2 + 2S$ (8)

where S is the adsorption sites on catalyst surface, and (a) denotes the adsorption state. The reaction process mainly includes three processes: the adsorption of reactant molecules, NO dissociation (rate-determining step)[45, 46], and desorption of production. The NO reduction by CO is a site-specific reaction wherein CO is molecularly adsorbed and NO is chemisorbed[47]. When exposing the CuSi catalyst to NO reaction gas at room temperature, NO molecules are adsorbed on the Cu^{2+} or Cu^0 of catalyst surface to generate several kinds of nitrate and nitrite species at room temperature, CO is adsorbed on the Cu^+ sites as Cu^+-CO[48] (Step (1) and Step (2)). The existence of Cu^0 could help to anchor more adsorbed NO. Two NO can bring together by migration to form ONNO (step (3)). Subsequently, adsorbed ONNO on Cu is easily dissociated into N_2O and O (Step (4)) during the heating process, especially for Cu^0[49-51]. When the CO molecules contact with NO pre-adsorbed CuSi catalyst, this dissociation is promoted dramatically and proceeded at lower temperature, meanwhile, CO can react with O to generate large amounts of CO_2 (Step (7)). At last, the generated N_2O (Step (5)), CO_2 (Step (7)), and N_2 (Step (8)) are desorbed from the catalytic surface.

4. Conclusions

In this study, the effect of preparation methods of CuO/SiO_2 on NO+CO reaction were investigated in depth. The catalyst prepared by ammonia-evaporation method (CuSi-AE) and impregnation method (CuSi-IM) displayed dispersed CuO and bulk CuO on SiO_2 support, respectively, and bulk CuO supported SiO_2 (CuSi-IM) presented excellent catalytic activity. By the exploration of the catalytic process, we clearly recognized that Cu^0 with a suitable crystallite size was the active site in CuO/SiO_2 catalysts. Since bulk CuO was more easily converted to Cu^0 than dispersed CuO in the reaction atmosphere, bulk CuO supported CuO/SiO_2 exhibited better performance in lower temperature. However, Cu^0 with large size are prone to agglomerate into larger particles in the reaction stream, which inhibits the catalytic performance due to the decrease in exposed active site. Combining various characterization, the results suggested that Cu^0 species played an important role in NO dissociation and the reaction between NO and CO.

Conflicts of interest

There are no conflicts to declare.

Acknowledgements

Financial support from the National Natural Science Foundation of China (21677069, 21773106, 21976081, 21972062), and Major Scientific and Technological Project of Bingtuan (2018AA002) are gratefully acknowledged.

Notes and references

1 K. Ueda, M. Tsuji, J. Ohyama, J. Ohyama and A. Satsuma, *ACS Catal.,* 2019, **9,** 2866-2869.
2 P. Granger and V. I. Parvulescu, *Chem. Rev.,* 2011, **111,** 3155-3207.
3 J. D. A. Bellido and E. M. Assaf, *Fuel,* 2009, **88,** 1673-1679.
4 D. Mantri and P. Aghalayam, *Catal. Today,* 2007, **119,** 88-93.
5 J. H. Holles, R. J. Davis, T. M. Murray and J. M. Howe, *J. Catal.,* 2000, **195,** 193-206.
6 H. S. Gandhi, G. W. Graham and R. W. McCabe, *J. Catal.,* 2003, 216, 433-442.
7 M. Iwamoto and H. Hamada, *Catal. Today,* 1991, **10,** 57-71.
8 D. I. Kondarides, T. Chafik and X. E. Verykios, *J. Catal.,* 2000, **193,** 303-307.
9 D. R. Wilburn and D. I. Bleiwas, *US Geol. Surv.,* 2004, **1224,** 2004-1224.
10 F. M. Auxilia, S. Ishihara, S. Mandal, T. Tanabe, G. Saravanan, G. V. Ramesh, N. Umezawa, T. Hara, Y. Xu, S. Hishita, Y. Yamauchi, A. Dakshanamoorthy, J. P. Hill, K. Ariga and H. Abe, *Adv. Mater.,* 2014, **26,** 4481-4485.
11 Y. Wang, A. Zhu, Y. Zhang, C. T. Au, X. Yang and C. Shi, *Appl. Catal. B: Environ.,* 2008, **81,** 141-149.
12 H. S. Gandhi and M. Shelef, *J. Catal.,* 1973, **28,** 1-7.
13 P. O. Larsson, A. Andersson, L. R. Wallenberg and B. Svensson, *J. Catal.,* 1996, **163,** 279-293.
14 L. Dong, L. Zhang, C. Sun, W. Yu, J. Zhu, L. Liu, B. Liu, Y. Hu, F. Gao, L. Dong and Y. Chen, *ACS Catal.,* 2011, **1,** 468-480.
15 X. Cheng, X. Zhang, D. Su, Z. Wang, J. Chang and C. Ma, *Appl. Catal. B: Environ.,* 2018, **239,** 485-501.
16 X. Wang, Y. Lu, W. Tan, A. Liu, J. Ji, H. Wan, C. Sun, C. Tang and L. Dong, *J. Colloid Interf. Sci.,* 2019, **554,** 611-618.
17 G. Centi and S. Perathoner, *Appl. Catal. A: Gen.,* 1995, **132,** 179-259.
18 L. Liu, Z. Yao, Y. Deng, F. Gao, B. Liu and L. Dong, *ChemCatChem,* 2011, **3,** 978-989.
19 C. Sun, J. Zhu, Y. Lv, L. Qi, B. Liu, F. Gao, K. Sun, L. Dong and Y. Chen, *Appl. Catal. B: Environ.,* 2011, **103,** 206-220.
20 T. Yamamoto, T. Tanaka, S. Suzuki, R. Kuma, K. Teramura, Y. Kou, T. Funabiki and S. Yoshida, *Top. Catal.,* 2002, **18,** 113-118.
21 X. Y. Jiang, L. P. Lou, Y. X. Chen and X. M. Zheng, J. Mol. *Catal. A: Chem.,* 2003, **197,** 193-205.
22 H. Iwamoto, S. Kameoka, Y. Xu, C. Nishimura and A. P. Tsai, *J. Phys. Chem. Solids,* 2019, **125,** 64-73.
23 M. Fernandez-Garcia, C. M. Alvarez, L. Rodriguez-Ramos, A. Guerrero-Ruiz and G. L. Haller, *J. Phys. Chem.,* 1995, **99,** 16380-16382.
24 R. T. Rewick and H. Wise, *J. Catal.,* 1975, **40,** 301-311.

View Article Online
DOI: 10.1039/D0CY00191K

25 A. Bienholz, H. Hofmann and P. Claus, *Appl. Catal. A: Gen.,* 2011, **391,** 153-157.
26 C. J. G. Van Der Grift, P. A. Elberse, A. Mulder and J. W. Geus, *Appl. Catal.,* 1990, **59,** 275-289.
27 M. Shimokawabe, N. Hatakeyama, K. Shimada, K. Tadokoro and N. Takezawa, *Appl. Catal. A: Gen.,* 1992, **87,** 205-218.
28 G. Diaz, R. Perez-Hernandez, A. Gomez-Cortes, M. Benaissa, R. Mariscal and J. L. G. Fierro, *J. Catal.,* 1999, **187,** 1-14.
29 Y. Chen and L. Zhang, *Catal. Lett.,* 1992, **12,** 51-62.
30 L. Liu, B. Liu, L. Dong, J. Zhu, H. Wan, K. Sun, B. Zhao, H. Zhu, L. Dong and Y. Chen, *Appl. Catal. B: Environ.,* 2009, **90,** 578-586.
31 S. Wang, X. Li, Q. Yin, L. Zhu and Z. Luo, *Catal. Commun.,* 2011, **12,** 1246-1250.
32 A. Yin, C. Wen, X. Guo, W. Dai and K. Fan, *J. Catal.,* 2011, **280,** 77-88.
33 L. Chen, P. Guo, M. Qiao, S. Yan, H. Li, W. Shen, H. Xu and K. Fan, *J. Catal.,* 2008, **257,** 172-180.
34 Z. Huang, F. Cui, H. Kang, J. Chen, X. Zhang and C. Xia, *Chem. Mater.,* 2008, **20,** 5090-5099.
35 J. Pike, S. W. Chan, F. Zhang, X. Wang and J. Hanson, *Appl. Catal. A: Gen.,* 2006, **303,** 273-277.
36 A. Gervasini, M. Manzoli, G. Martra, A. Ponti, N. Ravasio, L. Sordelli and F. Zaccheria, *J. Phys. Chem. B,* 2006, **110,** 7851-7861.
37 A. Auroux, A. Gervasini and C. Guimon, *J. Phys. Chem. B,* 1999, **103,** 7195-7205.
38 G. Wang, R. van den Berg, C. de Mello Donega, K. P. de Jong and P. E. de Jongh, *Appl. Catal. B: Environ.,* 2016, **192,** 199-207.
39 K. Hadjiivanov and H. Knözinger, *Phys. Chem. Chem. Phys.,* 2001, **3,** 1132-1137.
40 G. Centi, S and Perathoner, *Appl. Catal. A: Gen.,* 1995, **132,** 179-259.
41 O. Dulaurent, X. Courtois, V. Perrichon and D. Bianchi, *J. Phys. Chem. B,* 2000, **104,** 6001-6011.
42 X. Jiang, G. Ding, L. Lou, Y. Chen and X. Zheng, *J. Mol. Catal. A: Chem.,* 2004, **218,** 187-195.
43 X. Yao, F. Gao, Y. Cao, C. Tang, Y. Deng, L. Dong, Y. Chen, *Phys. Chem. Chem. Phys.,* 2013, **15,** 14945-14950.
44 M. Shimokawabe, N. Hatakeyama, K. Shimada, K. Tadokoro, N. Takezawa, *Appl. Catal. A: Gen.,* 1992, **87,** 205-218.
45 D. R. Rainer, M. Koranne, S. M. Vesecky, D. W. Goodman, *J. Phys. Chem. B,* 1997, **101,** 10769-10774.
46 Y. Xiong, X. Yao, C. Tang, L. Zhang, Y. Cao, Y. Deng, F. Gao, L. Dong, *Catal. Sci. Tech.,* 2014, **4,** 4416-4425.
47 S. Roy, M. S. Hegde, G. Madras, *Appl. Energ.,* 2009, **86,** 2283-2297.
48 X. Cheng, X. Zhang, D. Su, Z. Wang, J. Chang, C. Ma, *Appl. Catal. B: Environ.,* 2018, **239,** 485-501.
49 P. Li, L. Feng, F. Yuan, D. Wang, Y. Dong, X. Niu and Y. Zhu, *Catalysts,* 2016, **6,** 124.
50 L. Liu, Q. Yu, J. Zhu, H. Wan, K. Sun, B. Liu, H. Zhu, F. Gao, L. Dong, Y. Chen, *J. Colloid Interf. Sci.,* 2010, **349,** 246-255.
51 X. Zhang, X. Cheng, C. Ma, Z. Wang, *Catal. Sci. Technol.,* 2018, **8,** 3336-3345.

View Article Online
DOI: 10.1039/D0CY00191K

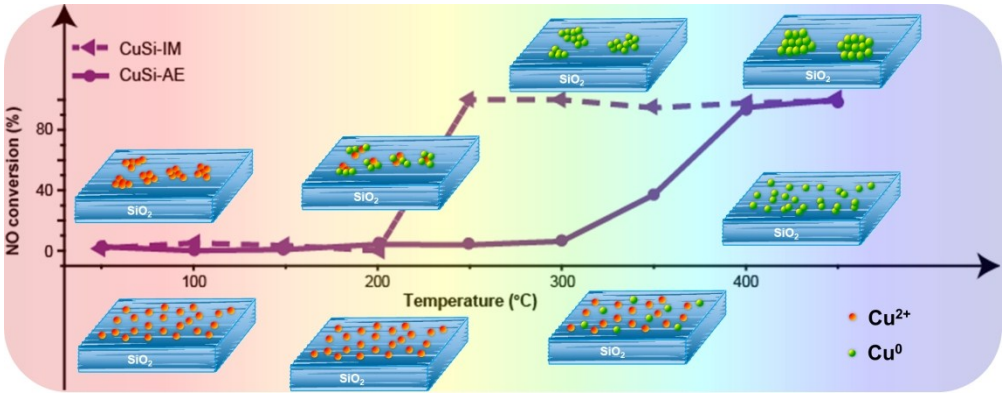

406x157mm (150 x 150 DPI)